Multiscale kinetic modeling of biomass fractionation in an experiment: understanding individual reaction mechanisms and cellulose degradation

Silabrata Pahari[a,b,*], Juhyeon Kim[a,b,*], Hyun-Kyu Choi[a,b], Mairui Zhang[c], Anqi Ji[c], Chang Geun Yoo[c], Joseph Sang-Il Kwon[a,b,**]

[a] *Artie McFerrin Department of Chemical Engineering, Texas A&M University, College Station, TX 77845 USA*
[b] *Texas A&M Energy Institute, Texas A&M University, College Station, TX 77845 USA*
[c] *Department of Chemical Engineering, State University of New York College of Environmental Science and Forestry, Syracuse, New York 13210, USA*

Abstract

To avoid over-consumption and wastage of virgin fibers, the quality of pulp products is as important as their productivity. To this end, both the quality and quantity of pulp should be considered together during the pulping processes. Multiple experimental studies have highlighted that maintaining a high degree of polymerization (DP) for cellulose microfibers in the wood chip ensures a good quality pulp product. However, in the pulping process, the applied reagents and severe conditions can cause a certain degree of cellulose degradation, accompanying unwanted lowering of fiber grades. In order to mitigate cellulose degradation during this step, it is crucial to control the process conditions such as reagent concentration and temperature. Also, to establish the optimum operating strategies, it is necessary to understand how the operating conditions impact the DP of cellulose microfibers. Therefore, we have proposed a novel multiscale model which predicts mesoscopic properties (*e.g.*, the lignin content and fiber morphology) alongside microscopic properties (*e.g.*, the DP of the cellulose microfibers). The proposed model incorporates a multi-layered kinetic Monte Carlo (kMC) framework that allows us to capture the temporal evolution of lignin content, fiber morphology, and cellulose DP, occurring at disparate

---

[*] The authors have contributed equally.

[**] Corresponding author

Email address: `kwonx075@tamu.edu` (Joseph Sang-Il Kwon)

timescales, as a function of reaction conditions in a computationally tractable fashion. Furthermore, the model predictions are validated with the experimental results so that it gives us a detailed picture of the pulp production processes. Overall with the proposed model, we aim to maximize productivity and maintain a high quality of cellulose fibers from the wood chips during the pulping process.

Keywords: Pulp digester; pulp quality; cellulose; glycosidic linkage; layered-kMC; multiscale modeling

---

1. Introduction

In recent years, the concern for the environment has grown across all the industrial sectors of the developed world. Like other industries that have high greenhouse emissions, the pulp and paper industry has made significant efforts to reduce its carbon footprint by optimizing resource consumption in the paper production process [1, 2]. Due to the stringent environmental constraints, the industry has primarily focused on reducing their feedstock consumption while improving paper quality via novel operating strategies [3, 4, 5]. While it requires a detailed understanding of the pulping process (i.e., the process by which the wood chips are converted to pulp used for making papers) to come up with such innovations, there is still a knowledge gap in regard to the comprehensive process information among the pulp and paper industries. To this end, both the industry and academia have put significant research efforts to develop mathematical models that can explain the pulping process and relate the process inputs to the properties of the paper produced [6, 7].

Woody biomass, the primary feedstock in the pulping process, is mainly composed of lignin, cellulose, and hemicellulose [8, 9]. Among these components, cellulose forms microfibers with a crystalline structure and determines the quality of the paper produced. Specifically, those microfibers are a primary building block and play an important role as one of the main load-bearing elements of the papers [10, 11, 12]. Therefore, they have extended their practical applications in the textile, construction, as well as polymer synthesis owing to their sustainable, inexhaustible, and regenerative nature [13, 14, 15]. The degree of polymerization (DP) of cellulose in the microfibers is significantly related to the quality of the paper produced including their tensile strength according to their structure-property relationships [16, 17]. That is, the improved quality of the generated paper is mainly attributed to the greater DP of the cellulose microfibers [18, 19]. During the pulping process (*i.e.,* the process where the wood chips are converted to the pulp), delignification is performed to separate lignin from the wood chip and to minimize lignin content in the fibers [20, 21]. However, the applied catalysts and solvents not only delignify the wood chips but also interact with cellulose fibers, and thus, it is unavoidable to reduce cellulose DP during the pulping process [22, 23].

During pulping process, Kappa number is used to measure the degree of delignification, and a low Kappa number implies that more lignin is removed from the bulk [24, 25]. It is to be noted that delignification is of great importance as the specific paper qualities (e.g., brightness) is determined by the amount of residual lignin. Hence, it is thought to be advantageous to add strong chemical reagents in order to accelerate reactions and minimize the Kappa number at the digester [26, 27]. Nevertheless, those reagents can stimulate undesirable cellulose degradation as they break down the glycosidic linkages of cellulose fibers [28]. These reactions must be avoided since they can drastically decrease cellulose DP, degrade the mechanical strength of paper, and also reduce the yield of pulp [29, 30, 31]. In this sense, it is critical to manage the operating conditions like the cooking temperature or time properly [32, 33]. Despite some knowledge already available about the relationship between pulping conditions and cellulose DP

[34, 35], it is still challenging to monitor the changes of cellulose DP simultaneously during the pulping process. Therefore, it would be beneficial to see how the input parameters (*i.e.*, operating conditions) can affect the cellulose quality through the use of a high-fidelity model (in a soft-sensor manner) and determine the optimal operating strategies.

As the entire pulping process is difficult to be elaborated in detail because of many interactions happening in tandem over various length and time scales, we present a multiscale model utilizing the kinetic Monte Carlo (kMC) approach [36, 37]. Specifically, multiscale events are captured on a simulation lattice where a layered-kMC approach is implemented to calculate mesoscopic properties like Kappa number and cell wall thickness (CWT) alongside microscopic properties like cellulose DP. The spatiotemporal evolution of the system's multiscale properties is acquired by executing multiple microscopic events in between succeeding macroscopic ones on simulation lattice sites. By doing this, we can obtain the long time-scale distributions of wood chip components in a computationally tractable manner while avoiding the insufficient sampling of slower dissolution reactions; so the multiscale model well predicts the temporal evolution of key pulp parameters including Kappa number and cellulose DP.

As presented in our previous study, 4-phenolsulfonic acid (PSA) treatment resulted in an effective cellulose fractionation from poplar wood chips under mild conditions [38]. Therefore, the multiscale model is built based on this process, and PSA pulping was conducted with Aspen wood chips in order to validate the proposed model. In this fashion, our results can offer a comprehensive picture of the cellulose degradation process. Additionally, because the suggested model is sensitive to reaction variables (*i.e.*, the process temperature and cooking time), it may be used to successfully manage the operating strategies that not only secure a target Kappa number but also enable an improved yield of cellulose with sufficient cellulose DP for paper production.

This article is arranged as follows: In the model formulation section, the details of the layered-kMC algorithm to capture the multiscale pulping process are presented; in this model, the details of the various kMC steps are highlighted. In the simulation section, the details of implementing this algorithm in the pulping process are highlighted. Subsequently, in the results and discussion section, the major findings from the proposed framework are presented. Lastly, in the conclusion section, a number of significant insights inferred from the simulation results are highlighted.

2. Model formulation

Throughout the wood chip treatment process, there are a number of key parameters which can be obtained by analyzing the different scales of interactions in the pulp digester. Hence, a multiscale model is developed in this work to depict the system in different length and time scales. To begin with, the continuum-scale mass and energy balance equations are used to describe the macroscopic changes. They determine the kinetics of the dissolution of major wood chip components (lignin, cellulose, and hemicellulose) or the mass and heat transfer. Subsequently, a layered-kMC model is implemented to capture the evolution of meso/microscopic properties using the simulation lattice. The model consists of two kMC layers (upper/lower layer), and two separate reactions are assigned to each layer. First, the upper layer utilizes the dissolution reaction rates, and it predicts where and how the dissolution reactions occur. As a result, the microconfiguration of the chip changes, and then the mesoscopic properties (Kappa number and CWT) are computed. Besides, the lower layer is introduced to simulate cellulose depolymerization taking place at a smaller scale. This layer provides us with the microscopic property (cellulose DP distribution) over the reaction time, completing the overall simulation dataset. The details of each layer and the working principles of the kMC simulation are discussed in the subsequent sections. It is notable that our multiscale approach not only integrates the different scales but enables taking a snapshot of the detailed configuration of a wood chip at a certain instance, beyond which can be described by the general mass/energy balances for a pulp digester.

2.1. Basic description of wood chip microstructure

The cell wall structure is mainly composed of three components: lignin, cellulose, and hemicellulose. Cellulose is a structural framework of the wood chip, and lignin and hemicellulose are the components surrounding cellulose and making inter-fiber connections. To produce high-quality cellulose products, delignification, the process of removing lignin from the wood chip [39, 40], is essential. However, during the delignification, the cellulose fibers also become exposed to the solvent and have a risk of unwanted degradation. Therefore, removing lignin content while preserving the quantity and quality of cellulose fibers has become the holy grail of the wood chip treatment processes. To this end, a high-fidelity model to predict cellulose degradation is proposed that can be employed to design the operating strategies required for the production of high-quality pulps [41, 42].

2.2. Macroscopic model

In the pulping processes, the wood chips are first fed into the solution with having certain porosity. As shown in Fig. 1, the entire system can be classified into three different phases. First, the solid phase includes the basic components of the wood chips consisting of lignin, cellulose, and hemicellulose. In addition, the liquor phase can be divided into two different regions. The

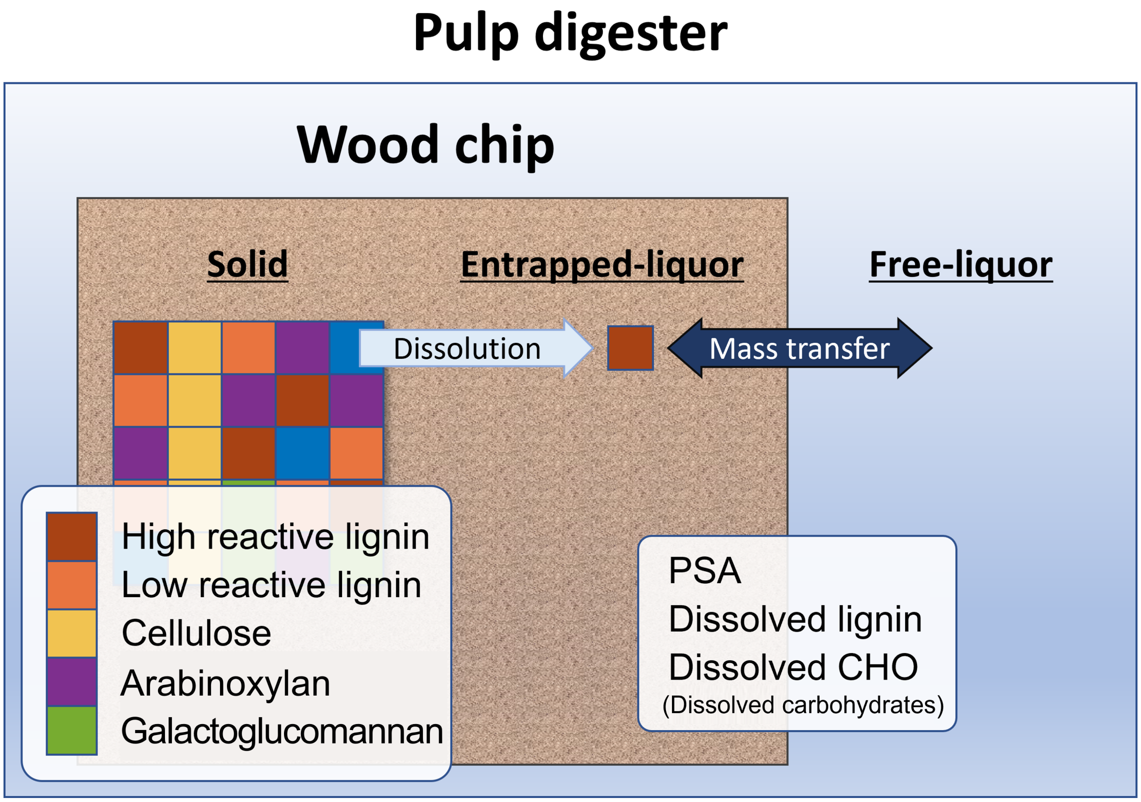

Fig. 1. The illustration of a pulp digester consisting of three phases (solid, entrapped-liquor, and free-liquor) with their components.

entrapped-liquor stands for the liquid portion residing in the wood chip pores, and they are able to interact with solid components. Meanwhile, the free-liquor phase is the liquid existing out of the chip. PSA is firstly fed into the digester as a solvent as well as a pulping reagent, and as the reaction proceeds, the lignin and other carbohydrate species (*e.g.*, cellulose and hemicellulose) are dissolved into liquor phase and become liquor phase constituents.

Once the wood chips are fed, the subsequent steps (*i.e.*, dissolution and degradation of cellulose) occur in three phases. During these interactions, the system parameters change accordingly through two layers of kMC simulation. Throughout this simulation, the macroscopic model sets the mass/energy balances which can figure out basic system information, such as temperature and concentrations. Here, the model also determines the rates of the mesoscopic interactions, and they are controlling the entire simulation in a realistic way. The details of the mass and energy balance equations are described in the following sections.

2.2.1. Mass balances

First, for the mass balances to be established, we have to track the concentration profiles of each component over reaction time. In this work, five components are considered in the solid phase, including high- and low-reactive lignin (s_1 and s_2), cellulose (s_3), and hemicellulose species, xylan (s_4) and glucomannan (s_5). As discussed earlier, the entrapped-liquor phase consists of PSA (e_1), dissolved lignin (e_2), dissolved carbohydrates (e_3) (*i.e.,* cellulose, and hemicellulose). As the free-liquor only undergoes mass transfer with the entrapped-liquor phase, the free-liquor phase also has the same constituents. It should be noticed that, during a series of dissolution reactions in this simulation, solid lignin and polysaccharides are converted to dissolved lignin and carbohydrates (*i.e.,* degraded and solubilized hemicellulose and cellulose oligosaccharides), respectively.

In this work, the concentration is calculated by Eq. 1:

$$C_{A_i} = \frac{\text{The mass component } i \text{ in the phase } A}{\text{The volume of phase } A} \quad \left[\frac{kg}{m^3}\right] \tag{1}$$

where the phase A can be s, e, and f for solid, entrapped-, and free-liquor phase, respectively.

Using the concentration defined above, the rate of dissolution and mass transfer can be set as a function of concentrations for each phase. First, for the solid phase, the rate of dissolution can be obtained as follows [43]:

$$r_{s_i} = V_s \frac{dC_{s_i}}{dt} = -V_s(k_{1,i}C_{e_1} + k_{2,i}C_{e_1}^{\frac{1}{2}}C_{e_3}^{\frac{1}{2}})(C_{s_i} - C_{s_i}^{\infty})^{\alpha} \quad \left[\frac{kg}{min}\right] \tag{2}$$

where V_s, $C_{s_i}^{\infty}$, and α stand for the solid phase volume, inert mass, and the reaction order, respectively. Here, $i = 1, \cdots, 5$ stands for high-, low-reactive lignin, cellulose, xylan, and glucomannan, respectively. Additionally, C_{e_j} stands for the concentration of the j^{th} species in the entrapped-liquor phase, where $j = 1, 2, 3$ for PSA, dissolved lignin, and carbohydrates, respectively. Furthermore, $C_{s_i}^{\infty}$ can be expressed in terms of the inert fraction, $\gamma_{s_i}^{\infty}$; hence, $C_{s_i}^{\infty} = \gamma_{s_i}^{\infty} C_{s_{i,0}}$. Also, the reaction rate constant, k_i, can be expressed as following the Arrhenius type equation:

$$k_i = A_i \exp\left(-\frac{E_{a,i}}{RT_c}\right) \tag{3}$$

From above, A and E_a are a pre-exponential factor and the activation energy to be estimated. R and T_c are the gas constant and the temperature of the chip phase; that is, the temperatures for solid and entrapped-liquor are considered identical. This will be explained with the energy balances in the following section.

The entrapped-liquor phase is the liquor present within the chip pore. As it is adjacent to both the solid surface and free-liquor, it plays an important role as the region where the dissolution of the solid components and the mass transfer take place. Therefore, in terms of the reaction kinetics, the mass balance considering both dissolution and mass transfer can be expressed as:

$$r_{e_j} = V_e \frac{dC_{e_j}}{dt} = V_e D(C_{f_j} - C_{e_j}) - V_c \sum_{i=1}^{5} b_{ji} r_{s_i} \quad \left[\frac{kg}{min}\right] \tag{4}$$

where V_e and V_c are the volumes of the entrapped-liquor and the chip phases. D is the average diffusivity for the liquors; and the empirical relationship between D and T_c is found in a previous study [44]:

$$D = 6.1321\sqrt{T_c} \exp\left(-\frac{4870}{1.98T_c}\right) \quad \left[\frac{1}{min}\right] \tag{5}$$

Also, b_{ji} is for the stoichiometric relationships between solid component i and liquor component j; this corresponds to the (j, i) element of the matrix B given in Eq. 6.

$$B = \begin{bmatrix} b_{11} & b_{12} & b_{13} & b_{14} & b_{15} \\ b_{21} & b_{22} & b_{23} & b_{24} & b_{25} \\ b_{31} & b_{32} & b_{33} & b_{34} & b_{35} \end{bmatrix} \tag{6}$$

Specifically, the interaction values of the solid components in the wood chips with entrapped liquor components (i.e, dissolved lignin, CHO, and PSA) are set as follows:

$$B = \begin{bmatrix} 0.185 & 0.185 & 0.49 & 0.49 & 0.49 \\ -1.0 & -1.0 & 0 & 0 & 0 \\ 0 & 0 & -1.0 & -1.0 & -1.0 \end{bmatrix} \tag{7}$$

The interaction parameters from dissolved lignin and -CHO are obtained from [26]. Furthermore, it is assumed that the interaction strengths of Active Alkali and PSA in dissolving wood chip components are comparable in the pulp digester. Therefore, we considered the interaction strengths of Active Alkali and PSA to be the same. It is to be noted that the free-liquor phase is the liquor fraction not being caught by the chip pores. Assuming that the solid-liquor interactions only occur in the entrapped-liquor phase, the free-liquor concentrations are only affected by the mass transfer. Hence, the mass balance for the free-liquor becomes:

$$r_{f_j} = V_f \frac{dC_{f_j}}{dt} = V_f \left(D \frac{\epsilon V_c}{V_f} \left(C_{e_j} - C_{f_j} \right) \right) = D \epsilon V_c \left(C_{e_j} - C_{f_j} \right) \quad \left[\frac{kg}{min} \right] \tag{8}$$

where ϵ is the porosity of the wood chip, *i.e.*, V_e/V_c; thus, the added term, $\epsilon V_c/V_f$ $(= V_e/V_f)$ renders the rate equation as a function of the free-liquor phase volume. Note that, the porosity ϵ

is defined at Eq. 13; it is updated at every time segment and used for mass balance calculation.

Finally, the mass transfer rate between the liquor phases can be set as:

$$r_m = D \sum_{j=1}^{3} \left(\left| C_{e_j} - C_{f_j} \right| \right) (V_e + V_f) \quad \left[\frac{kg}{min} \right] \tag{9}$$

where V_f stands for the free-liquor volume. The absolute value sign determines the direction of the mass transfer, which is driven by the concentration gradient.

Here, it is to be noted that the kMC simulation lattice is primarily utilized to explain the spatiotemporal evolution of the chip phase. In detail, dissolution of the wood chip components are explained by the chip phase mass balance (Eq. 2); the corresponding kMC lattice site is filled with the liquor phase. Although the mass balances for both liquor phases (Eq. 4 and 8) are not directly related to the kMC lattice, they are still considered since those impact the overall reaction propensity. For a deeper understanding, the algorithm is further elaborated in the Sect. 2.3.

2.2.2. Energy balances

Apart from the concentration profile of each component, the system temperature is also supposed to be controlled, since the temperature influences diverse aspects of the reaction, from the reaction rates to the process safety.

As mentioned before, the temperatures of the solid and entrapped-liquor phases are remained the same and set as one variable, the wood chip temperature, T_c. As the chip phase temperature is influenced by the bulk dissolution as well as the mass transfer, the energy balance for the wood chip can be expressed as below:

$$\left(c_{p_s} M_s + \epsilon c_{p_e} M_e\right) \frac{dT_c}{dt} = \Delta H_R \sum_{i=1}^{3} r_{s_i} + U\left(T_f - T_c\right) + D\epsilon d_E \tag{10}$$

where c_{p_s} and c_{p_e} are the heat capacities of the solid and entrapped-liquor phases, respectively. Also, M_s and M_e are the total masses of the solid and entrapped-liquor phases, respectively. ΔH_R is the heat of reaction, T_f is the free-liquor phase temperature, U is the overall heat transfer coefficient, and d_E is the amount of energy transferred from the free-liquor to the solid phase by diffusion.

In the same way, the energy balance for the free-liquor becomes:

$$c_{p_f} M_f \frac{dT_f}{dt} = U\left(T_c - T_f\right) + D\frac{\epsilon V_c}{V_f} d_E \tag{11}$$

where M_f and c_{p_f} are the total mass and the heat capacity of the free-liquor phase. As both the liquor phases consist of the dissolved solid components and liquors, the liquor heat capacities can be determined using the following relationships:

$$\begin{aligned} c_{p_e} &= c_{p_s} x_{es} + c_{p_l} x_{el} \\ c_{p_f} &= c_{p_s} x_{fs} + c_{p_l} x_{fl} \end{aligned} \tag{12}$$

where c_{p_l} is the heat capacity of the liquor, which is supposed to be the same as the heat capacity of the PSA solution, and x_{ab} is defined as the mass fraction of the b-phase component being dissolved or existing in the phase a.

2.3. Mesoscopic model description (the upper kMC layer)

To perform a multiscale simulation, the constituent components for each phase are defined as exhibited in Fig. 1. Then, the system properties, such as concentration/temperature profile, are computed based on the mass/energy balance equations as mentioned in Section 2.2.

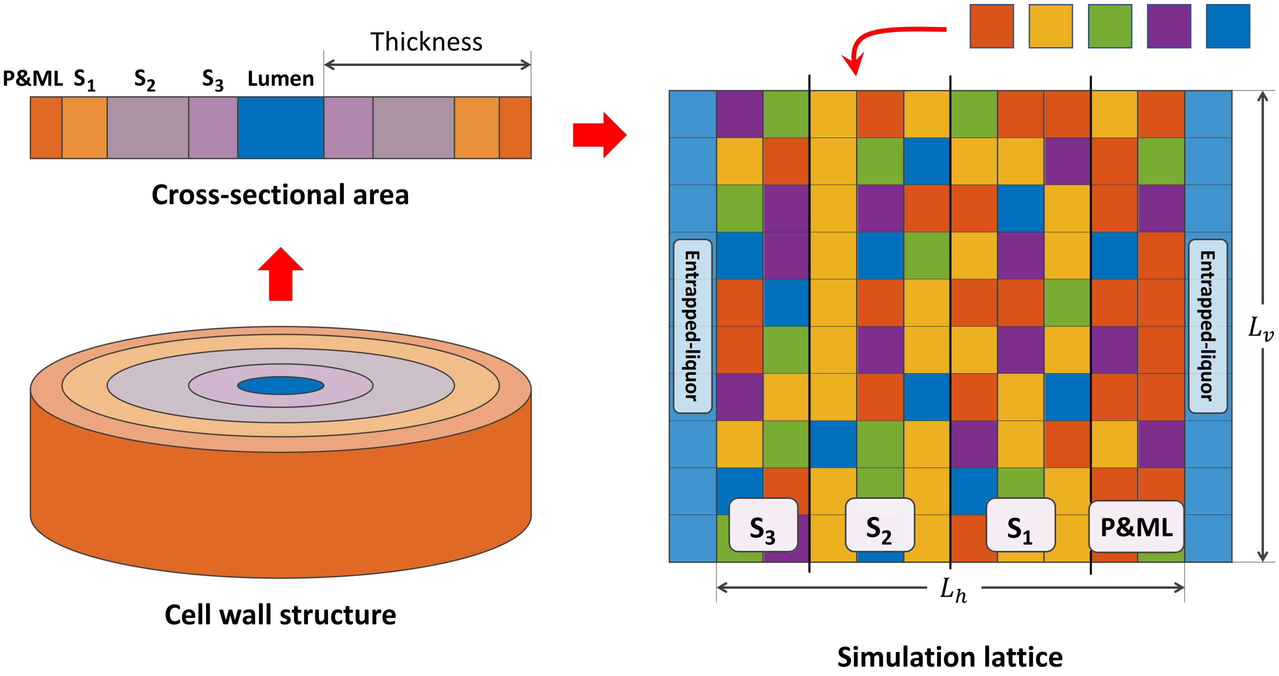

Fig. 2. The illustration of the simulation lattice.

Here, the biomass configuration is represented as a simulation lattice that enables us to capture the spatiotemporal variation in the concentration of the different wood chip components during the dissolution phenomena [24, 26, 44]. As exhibited in Fig. 2, a two-dimensional axisymmetric simulation lattice is introduced here. The simulation lattice consists of four layers, *i.e.*, primary wall and middle lamella (P&ML), and three secondary wall layers (S_1, S_2, and S_3). This layer-wise representation ensures that the realistic structure of the wood chips gets captured in the proposed model. The initial composition of the components is kept according to that found in the Aspen wood chips and is also shown in Table 1.

Table 1. Chemical composition of the cell wall [45, 46]

	Lignin	Cellulose	Hemicellulose
P&ML	8.4 (80%)	0.7 (7%)	1.4 (13%)
S_1	10.5 (52%)	6.1 (30%)	3.7 (18%)
S_2	9.1 (15%)	32.7 (54%)	18.4 (31%)
S_3	0.0 (0%)	0.8 (13%)	5.2 (87%)
Total	28.0 (29%)	40.3 (41%)	28.7 (30%)

Since the diameter of dissolved lignin and cellulose elementary fibril is considered to be 3.5 nm [44], the length of a single lattice site is set as 3.5 nm. The size of the two-dimensional lattice is defined as the product of the number of horizontal and vertical lattice sites, $L_h \times L_v$. Here, $L_h = 3.8\mu m/3.5nm = 1086$ as the average thickness of the wood fibers is 3.8 μm; and L_v is set to be 800 representing the cell wall length. The solid and liquor components are assigned to each lattice site according to the initial chip porosity ($\epsilon_0 = 0.64$) and compositions for each cell wall layer on the basis of Table 1. The porosity is defined below and tracked at each time step during the simulation:

$$\epsilon = \frac{n_e}{L_h \times L_v} \tag{13}$$

where n_e is the number of lattice sites that are unoccupied by solid components, and $L_h \times L_v$ is the overall dimension of lattice sites explained earlier.

As the simulation lattice can provide the wood chip component accessibility to the entrapped-liquor during the dissolution reactions, it helps us predict where the dissolution is likely to occur and enables accurate tracking of the microscopic properties of the system. To elaborate in detail, the dissolution happens at the lattice site neighboring to the liquor; therefore, the algorithm randomly picks one liquor site first and evaluate the dissolution rates of the neighboring components based on the macroscopic mass balance equations. Then, utilizing those rates at every time instant, the probabilities for each of the dissolution or mass transfer events to be selected are calculated based on the ratio of each individual event over the sum of overall reaction rates ($r_{t,upper} = \Sigma r_{s_i} + r_m$). Then, a random number, $\xi_{p_1} \in (0, 1]$, is generated to determine which event is going to happen. As the probabilities (Table 6) are computed for each site, the corresponding component is dissolved out or mass transfer takes place. Subsequently, the time advancement for the executed event is computed by the following equation with another random number generated, $\xi_{t_1} \in (0, 1]$:

$$\Delta t_1 = - \sum_{\text{selected sites}} \frac{\ln \xi_{t_1}}{r_{t,upper}} \quad [min] \tag{14}$$

where $r_{t,upper}$ is the sum of all the reaction rates in the upper layer. These steps are repeated until the system reaches the predefined reaction time, 10, 20, and 30 minutes.

Table 2. The probability distribution for bulk dissolution reactions [47].

Probabilities	Phenomena
	Dissolution of:
$0 < \xi_{p_1} \leq \frac{r_{s_{ju}}}{r_{t,upper}}$	upper
$\frac{r_{s_{ju}}}{r_{t,upper}} < \xi_{p_1} \leq \frac{r_{s_{ju}}+r_{s_{jd}}}{r_{t,upper}}$	lower
$\frac{r_{s_{ju}}+r_{s_{jd}}}{r_{t,upper}} < \xi_{p_1} \leq \frac{r_{s_{ju}}+r_{s_{jd}}+r_{s_{jl}}}{r_{t,upper}}$	left
$\frac{r_{s_{ju}}+r_{s_{jd}}+r_{s_{jl}}}{r_{t,upper}} < \xi_{p_1} \leq \frac{r_{s_{ju}}+r_{s_{jd}}+r_{s_{jl}}+r_{s_{jr}}}{r_{t,upper}}$	right
	of the selected liquor site
$\frac{r_{s_{ju}}+r_{s_{jd}}+r_{s_{jl}}+r_{s_{jr}}}{r_{t,upper}} < \xi_{p_1} \leq 1$	Mass transfer

In every time step when a segment of cellulose is dissolved from the wood chips, there is an associated degradation in the DP of cellulose calculated in the model. Specifically, this degradation is captured by reducing the total number of $n_{cellulose}$-mers from randomly chosen cellulose chains in the wood chips. Here, $n_{cellulose}$ is the number of cellulose lattice units dissolved in the kMC simulation. This is the first mechanism via which cellulose degradation takes place.

As the dissolution reaction proceeds, the system variables like concentration and tempera-

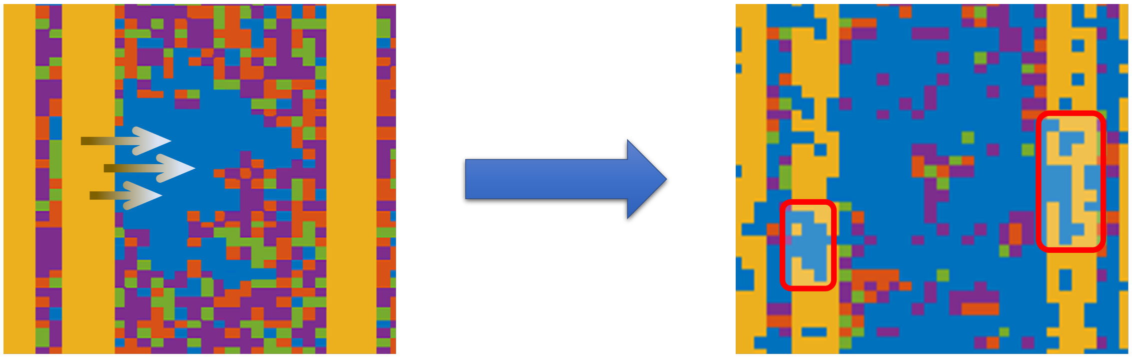

Fig. 3. The schematic illustration of the cellulose depolymerization mechanisms.

ture are correspondingly updated based on the mass and energy balance equations mentioned in the macroscopic model.

2.4. Microscopic model description (the lower kMC layer)

The governing equations in the previous section describe the evolution of mesoscopic properties and refer to the steps captured in the upper layer of the kMC simulation. Apart from the bulk dissolution reactions, as mentioned before, the cellulose fibers exposed to the liquor experience further degradation due to depolymerization; this reaction takes place in the form of hydrolysis. It is to be noted that the mesoscopic dissolution and microscopic depolymerization are significantly influenced by the system parameters like temperature, and reaction rates. However, being a microscopic intramolecular reaction, cellulose depolymerization occurs at a different length and time scale as compared to bulk dissolution reactions. To account for this fact, the second kMC layer for depolymerization is placed within the existing one. Therefore, these multiscale reactions must be considered together. For the microscopic model, the lower layer of the kMC algorithm is implemented to capture the following aspects of the microscopic properties of the system: the temporal evolution of cellulose DP distribution, and its sensitivity

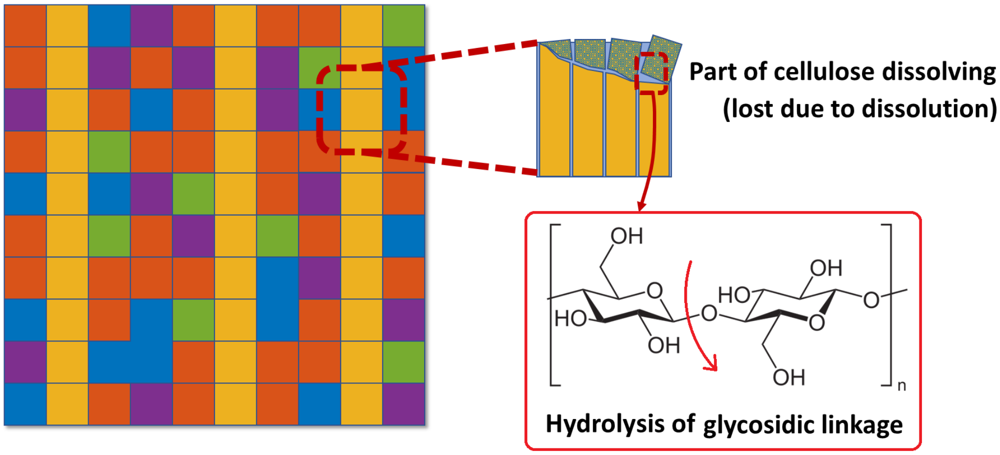

Fig. 4. Mechanism for cellulose degradation during the pulping process, specifying two important phenomena governing cellulose degradation.

to various reaction conditions.

It is to be noted that the bulk dissolution reactions involve mass losses as the biomass components are dissolved out. Fig. 3 displays the illustration of the cellulose fiber degradation. The fibers are depolymerized to smaller fractions. In the figure, the yellow masses stand for a bunch of the cellulose fibers, and the lattice sites adjacent to the liquor dissolved out. Then, in the microscopic layer, the bond within the fiber is broken. Cellulose depolymerization is mostly caused by the cleavage of its glycosidic linkages and results in cellulose DP distribution over the reaction time. So it does not make the apparent changes in the simulation lattice, because it is different from the bulk dissolution, but the chain lengths of the individual cellulose fiber decreases; this is illustrated in Fig. 4. During the kMC simulation, the cellulose DP distribution is calculated considering these two cellulose degradation mechanisms exhibited in both Figs. 3-4.

In this study, the depolymerization is also explained by the aforementioned simulation lattice and the followings are assumed: (1) Glucose, a monomeric form of cellulose, has a molecular size of 1 nm; (2) while depolymerization takes place, any kind of repolymerization will not happen; (3) the cellulose degradation is the first-order reaction; (4) the system temperature and pressure do not change as a result of cellulose degradation; and (5) the probabilities of breakage are all the same for every scission point.

The cellulose depolymerization kinetics for a fiber whose DP is L follows the rate law below:

$$r_d = -k_d(L-1)p_L \tag{15}$$

where p_L stands for the number fraction of L-mers in the system. Here, the rate constant for the degradation is also in the Arrhenius form:

$$k_d = A_d \exp\left(-\frac{E_d}{RT_c}\right) \tag{16}$$

where A_d and E_d are the pre-exponential factor and the bond dissociation energy for the depolymerization, respectively. The other intra-/inter-molecular reactions are also present in the depolymerization kinetics. Peeling-off is the end-chain scission reaction, which removes one monomer from either end of the polymer chain. Also, stopping is to make the polymer chain stable and inactive to further de/repolymerization reactions. Those two are regarded as null reactions so that they do not alter the degree of polymerization in this simulation, and are expressed as zeroth-order reactions:

$$r_{poly} = -(r_{peel} + r_{stop}) = -(k_{peel} + k_{stop}) \tag{17}$$

For simultaneous degradation, the total rate can be found as follows:

$$r_{t,lower} = r_{d,avg} + r_{poly} \tag{18}$$

where $r_{tot,lower}$ is the total rate of the reactions at the lower layer of kMC simulation, and $r_{d,avg}$ is the average rate of degradation reactions happening at the same time. Then, events for each cellulose fiber are again selected by using a random number, $\xi_{p_2} \in (0, 1]$, and the probabilities and the corresponding events are presented in Table 3.

Table 3. The probability distribution for cellulose depolymerization.

Probabilities	Depolymerization mechanism
$0 < \xi_{p_2} \le \frac{r_d}{r_{t,lower}}$	Random scission
$\frac{r_d}{r_{t,lower}} < \xi_{p_2} \le 1$	Peeling or stopping

While degradation proceeds, the time evolution is calculated in the same way as that of dissolution using a random number, $\xi_{t_2} \in (0, 1]$:

$$\Delta t_2 = -\frac{\ln \xi_{t_2}}{r_{t,lower}} \quad [min] \tag{19}$$

The microscopic events repeat until a series of Δt_2 accumulates to the mesoscopic time segment, Δt_1, with corresponding concentration and temperature updates.

2.5. Integrating kMC and continumm models

To couple the kMC simulation for the solid phase with the continuum mass and energy balance equations for the entrapped- and the free-liquor phases, information regarding the mass dissolved, change in porosity of the wood chips, kMC time increment associated with the upper kMC loop, and the time increment associated with the lower kMC loop is passed. Then, the continuum mass and energy balance equations are solved using the explicit Euler's method.

The process begins with the execution of the upper kMC loop, which provides the mass of the solid dissolved, the change in porosity of wood chips, and the time increment associated with the upper layer of kMC simulations. Subsequently, the lower kMC loop is performed, and as the event of depolymerization of cellulose fiber is executed, the time increment associated with the lower kMC loop is obtained. Finally, the change in the concentration of the solid associated with the time increment of the lower kMC loop is updated using Eq. 20, which is as follows:

$$C_{s_i}(t+\Delta t_2) = C_{s_i}(t) - \frac{M_k \Delta t_2}{V_s \Delta t_1} \tag{20}$$

where $C_{s_i}(t)$ is the concentration of the solid component i in the solid phase at time instant t, M_k is the mass of the dissolved lattice site k in the upper kMC loop, Δt_1 is the time step of the upper kMC loop, V_s is the volume of the solid phase, and Δt_2 is the time increment in the lower kMC loop. Using information obtained from the kMC simulations, the concentration of individual species in the entrapped liquor is obtained using Eq. 21, which is as follows:

$$C_{e_j}(t+\Delta t_2) = C_{e_j}(t) + \sum_{i=1}^{5} \frac{M_k \Delta t_2}{\epsilon V_s \Delta t_1} b_{ji} + D(C_{f_j}(t) - C_{e_j}(t))\Delta t_2 \tag{21}$$

where $C_{e_j}(t)$ is the concentration of the entrapped-liquor component j, $C_{f_j}(t)$ is the concentration of the free-liquor component j, $\epsilon(t)$ is the porosity of the wood chip at time t, D is the diffusivity of solid from the entrapped-liquor to the free-liquor, and b_{ji} is the stoichiometry of a solid component i in the liquor phase j. The porosity of the wood chip is obtained as follows:

$$\epsilon(t+\Delta t_1) = \epsilon(t) + \frac{\Delta\epsilon \Delta t_1}{\Delta t_2} \tag{22}$$

where $\Delta\epsilon$ is the total change in porosity of the wood chips in the upper layer of the kMC simulation. Then, the concentration of the components in the free-liquor is updated as follows:

$$C_{f_j}(t+\Delta t_2) = C_{f_j}(t) + D(C_{e_j}(t) - C_{f_j}(t))\Delta t_2 \tag{23}$$

In summary, the continuum mass balance equations for the entrapped- and free-liquor phases are solved forward in time with the explicit Euler's method. The mass of the solid dissolved, the change in porosity, and the time increment are obtained from the upper kMC layer, while the time increment associated with the lower kMC layer is also utilized in solving the continuum mass balance equations. This shows how both of the kMC layers are coupled with the continuum mass balance equations.

The temperature of the system is calculated by solving the following continuum energy balance equations:

$$T_c(t+\Delta t_2) = T_c(t) + \frac{\left(\frac{M_k}{\Delta t_1}\Delta H_R + U(T_f(t) - T_c(t)) - D d_E \epsilon(t)\right)\Delta t_2}{c_{p_s} C_s(t) V_s + c_{p_e} C_e(t) V_e \epsilon(t)} \tag{24}$$

where $T_c(t)$ is the chip phase temperature at a time instant, $T_f(t)$ is the free liquor temperature at a time instant, ΔH_R is the heat of reaction for the dissolving species, U is the overall heat-transfer coefficient, c_{p_s} is the specific heat capacity of the solid, c_{p_e} is the specific heat capacity of the entrapped liquor, d_E is the energy loss due to diffusing components from the entrapped liquor, $C_s = \sum_{i=1}^{5} C_{s_i}(t)$ is the overall concentration of the solid, and $C_e = \sum_{j=1}^{3} C_{e_j}(t)$ is the total concentration of the dissolved components in the entrapped-liquor. The free-liquor temperature is also obtained using the explicit Euler's method as follows:

$$T_f(t+\Delta t_2) = T_f(t) + \frac{U(T_c(t) - T_f(t)) + D\epsilon(t)\frac{V_c}{V_f} d_E}{c_{p_f} C_f(t) V_f} \tag{25}$$

where c_{p_f} is the specific heat capacity of the free-liquor phase, and $C_f(t) = \sum_{j=1}^{3} C_{f_j}(t)$ is the total concentration of the dissolved solid in the free-liquor phase.

Remark 1: *To obtain the temporal profiles of two values, the mass of a dissolved component from the solid phase and the number fraction of cellulose chains with a specific length, kMC simulations are conducted for both the dissolution and depolymerization reactions. The amount of components dissolved from the solid phase is equal to the amount of components received by the liquor phase. Once the amount of dissolved components is determined from the kMC simulation, it becomes crucial to use this information in the mass balance equations for the entrapped and free-liquor phases. This is necessary to describe how the distribution of dissolved components changes with time in both the phases.*

3. Simulation section

This section will give the overall scheme of the multi-layered kMC simulation and explain the details for each layer of this simulation. First, it shows how the macroscopic continuum model is integrated with the discrete event-based layered kMC simulations. As mentioned in the previous section, mesoscopic variables like Kappa number and CWT are obtained from the upper layer of the kMC simulations while the microscopic properties like the cellulose DP are obtained from the lower layer of the kMC simulations [24, 26]. Furthermore, the following paragraph explains how the kMC simulation captures the spatiotemporal evolution of the system's meso/microscopic properties. In this work, Matlab R2019a is particularly used for the kMC simulation.

Owing to the initial contact between the solid and liquor components, the liquor from the free-liquor phase enters the pores and becomes the entrapped-liquor components. The mass transfer rate is found by Eq. 9. Subsequently, the dissolution of the solids takes place and the rate constants for this dissolution are calculated from the literature. Since the dissolution is an action of etching of the wood chip components by PSA, the exposed area of the wood chip to the entrapped liquor remarkably affects how the wood chip morphology changes with time. In this work, the discrete event-based kMC simulation allows us to explicitly track the solid-liquor interface by keeping a list of lattice surface sites of solid components exposed to the entrapped-liquor phase. Here, it must be emphasized that the lattice sites having more faces exposed to the entrapped-liquor have a higher dissolution probability. Having the list of sites to be dissolved and dissolution probabilities, the dissolution rates are computed for the individual interfacial sites in the kMC simulation lattice. Implementing kMC simulations in this unique fashion allows us to capture the variation in the status of the system accurately. Associated with the mass transfer and dissolution, the temperature change takes place based on the energy balance equations (Eqs. 10-11). The temperature change alters the reaction rates of all the kMC events and consequently drives the key system variables to particular values. The temperature also impacts the depolymerization rate in the cellulose nanofibers, which finally affects the cellulose DP. This coupled process is conveniently captured by the layered-kMC simulation.

Table 4. Overall summary of the operating conditions [26]

Conditions	Values	Units
Wood chip thickness	0.8/3.0/5.0	mm
Dimension of simulation lattice site ($L_h \times L_v$)	1086×800	N/A
Dimension of a lattice site	3.5×3.5	mm^2
Treatment time (T_{fin})	10/20/30	min
Initial porosity (ϵ_0)	0.64	N/A
Initial system temperature	343/353/363	K
Heat capacities of:		
solid phase (C_{p_s})	1.47	$kJ/kg \cdot K$
pure liquor (C_{p_l})	4.19	$kJ/kg \cdot K$
Heat of reaction (ΔH_R)	-581	kJ/kg
Heat transfer coefficient (U)	827	$kJ/min \cdot K \cdot m^3$
Initial DP of the cellulose fibers	900	N/A

Table 5. Kinetic parameters for the dissolution reaction [48]

Parameters	Solid component indices (i)					Units
	1	2	3	4	5	
Pre-exponential factors						
$A_{1,i}$	0.3954	1.457×10^{11}	28.09	7.075	5.8267×10^{3}	$m^3/kg \cdot min$
$A_{2,i}$	12.49	1.873	124.9	47.86	3.225×10^{16}	

Table 6. The activation energy and rate constants for the three reactions for the cellulose polymers [49]

Parameters	Values
Activation energy for depolymerization of cellulose	62.031 $kJ/mol \cdot K$
Activation energy for peeling-off reactions	43.64 $kJ/mol \cdot K$
Activation energy for stopping reactions	54.44 $kJ/mol \cdot K$
Rate constant for hydrolysis reaction	4.906×10^{6} s^{-1}
Rate constant for peeling-off reaction	1.0937×10^{6} s^{-1}
Rate constant for stopping reaction	2.97×10^{7} s^{-1}

In the upper layer of the kMC simulation, the macroscopic state of the system like the temperature, and concentration are initialized. The overall simulation parameters and detailed operating conditions are summarized in Table 4. Subsequently, the dissolution rate for each face of the simulation lattice is obtained. For the reaction rates to be determined, the reaction rate constants need to be specified (Eq. 3); and the kinetic parameters are listed in Table 5. It is necessary to adjust the parameters of the high-fidelity model so that it fits well with the observed experimental data. The results for fitting the activation energies are highlighted in the results and discussions section. Then, based on the laws laid down in Table 6, faces are chosen for dissolution. It is to be noted that the n_{dis} number of lattice sites having the chosen configuration for the faces is dissolved at once: this parameter is set to 1000. Here, the dissolution events are simulated in the form of replacing the dissolved lattice sites with the liquor lattice sites. Once the dissolution event is executed, the time increment of the simulation system is computed from Eq. 14.

Furthermore, some portions of the cellulose nanofibers get degraded in tandem with the dissolved events. Once the cellulose sites are selected to be dissolved, the dissolving portions are removed, and cellulose DP is updated accordingly. Specifically, for each lattice site, the l_1 segments of the polymer chains are removed and the DP is updated. Here, l_1 is a ratio of the length of one single cellulose molecule to the length of one simulation lattice. From the literature [50], the size of a cellulose molecule is obtained to be 2.50 Å, while the size of a simulation lattice is 3.5 nm; and therefore, the value of l_1 is 14. The removal of polymer segments leads to a reduction in the cellulose DP. The decrease in cellulose DP due to the breakage of the glycosidic linkages is also important, and it is captured by the lower layer of the kMC simulation. In the upper layer of the kMC simulation, the time is advanced by δt_1, which is obtained from Eq. 14.

In the lower layer of kMC simulations, the microscopic process of breaking the glycosidic linkages is captured. In the lower layer of kMC simulations, the microscopic process of breaking the glycosidic linkages is captured. As observed from the values of the activation energies highlighted in Table 6, the activation energy (*i.e.*, cellulose depolymerization) is high. This makes the reaction very sensitive to temperature changes. Therefore, capturing the incremental changes in the system temperature due to mass transfer is crucial throughout the depolymerization process. To this end, the temperature change is captured by a set of steps. In the first step, the temperature value at the initial state for the upper layer of the kMC simulation is considered to calculate the depolymerization rate of cellulose. To mimic the process of depolymerization, a set of 1500 glucose molecules (each having 900 monomers) is considered and the random point scission mechanism is followed [37]. Then, the time step is increased using Eq. 19, and the total time spent in the lower layer of the kMC simulations is updated. Subsequently, the mass transfer taking place during this time interval is obtained from Eq. 2. Henceforth, the temperature change corresponding to this mass transfer is calculated via Eqs. 10-11. Finally, the temperature changes and the overall rate of the reaction are updated. This process is continued until the total time increment in the lower layer of the kMC simulation reaches one time step of the upper layer. The schematic of the two-layer kMC approach is displayed in Figs. 3-4.

In our layered-kMC approach, the reactions in two different scales are coupled, and a brief schematic for our layered-kMC simulation is summarized in Fig. 5. Using MATLAB R2019a, we implemented the code for kinetic Monte Carlo simulations and the manuscript showcases the results obtained from our implementation.

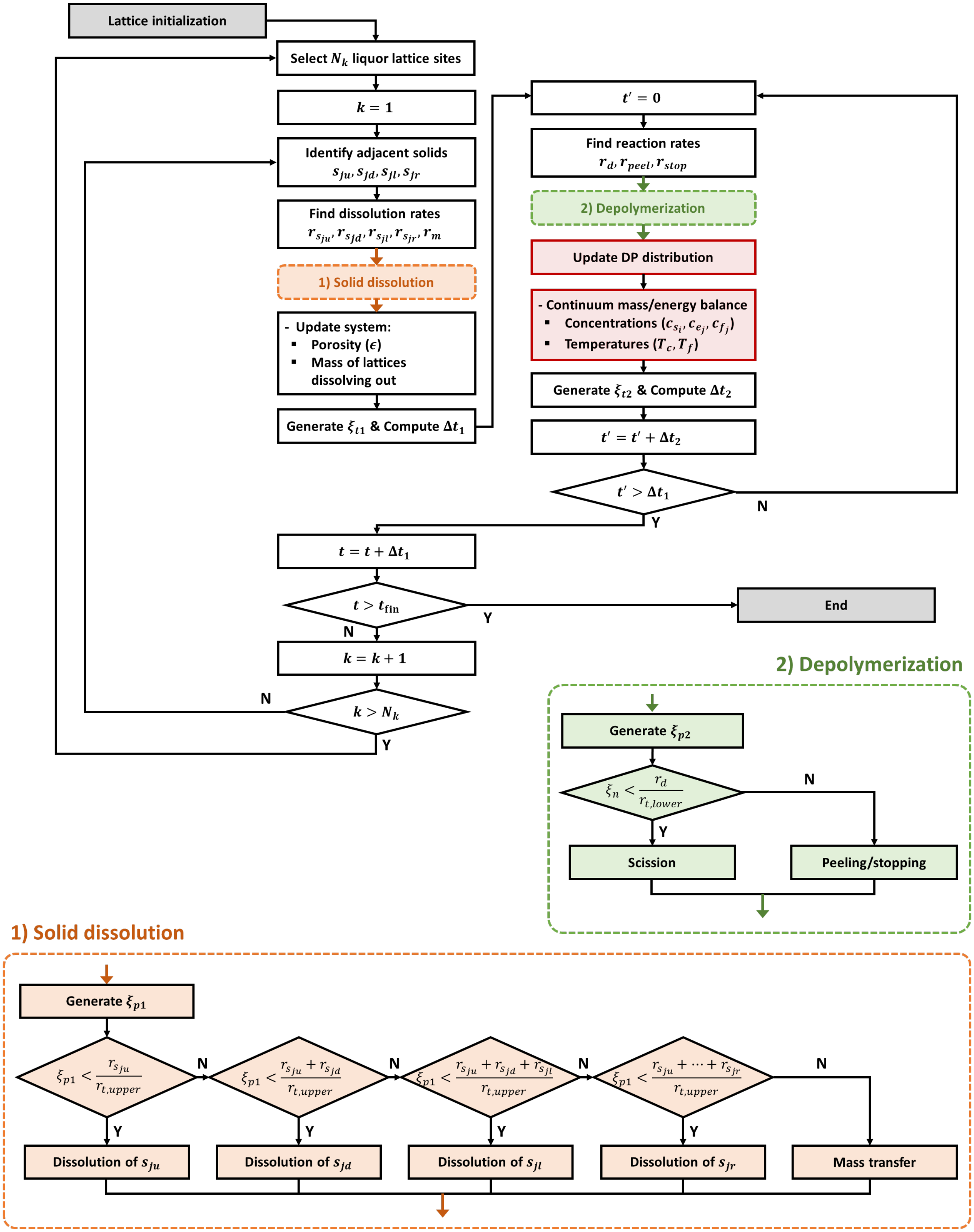

Fig. 5. The flowchart for the layered-kMC simulation algorithm.

4. Results and discussion

In this section, details of the various properties obtained from the layered-kMC simulations are highlighted. Specifically, the temporal variations of the important mesoscopic properties (*e.g.*, CWT and Kappa number) alongside the important microscopic properties (*e.g.*, DP of cellulose fibers) are calculated and presented in the following sections. The results reveal the effect of solution conditions like temperature and alkali concentration on the mesoscopic and microscopic properties of the wood chips.

4.1. Validation of the layered-kMC simulations

In order to utilize the proposed layered-kMC model as a digital twin of the depolymerization of cellulose, the model predictions are validated with the experimental data at two different temperatures as shown in Fig. 6. It is to be noted that the experiments are performed at temperatures of 345 K and 355 K, which are close to the temperatures at which the actual pulping process is carried out.

The experimental data are found to fit the model predictions well as shown in Fig. 6. However, minor discrepancies are observed; those might be attributed to the uncertainty associated with wood chip characteristics. The preparation procedures for the wood chips utilized in this study have the potential to create data inconsistencies. Specifically, our experiment involved conducting separate experiments with new batches to acquire individual data points for each time point (i.e., 15, 20, 25, 30 minutes) due to the time required for DP data sampling preventing us from running the reaction continuously. Nevertheless, it is important to note that even under the same experimental conditions, the wood chip characteristics may vary between batches, resulting in inconsistencies in the DP data. Moreover, it is worth noting that 1 mm size wood chips may have a greater degree of size variation than other sizes due to limitations in the milling and sieving procedure, which cannot accurately control the small size. On the other hand, the 3 and 5 mm size wood chips were prepared by manual cutting. As a result, the use of small size chips and distinct preparation methods could potentially lead to less consistent results. To achieve satisfactory agreements between simulations and the experiment, some modifications are necessary by making small changes to the parameters associated with wood properties (*i.e.*, effectiveness factor, inert fraction, etc.) depending on the age and species of the wood chip.

The good validations of the DP for the cellulose fibers at different temperatures indicate that the mechanism captured by the model is accurate so that the model can be used to predict important microscopic and mesoscopic properties. It is to be noted that the number-average degree of polymerization is utilized for the validation of experimental data. Specifically, owing to the higher central tendency of the number average molecular weight than the weight average molecular weight, it has been utilized in this study. This is due to the fact that, during calculations, the molecular weight of oligomers is not weighted with any factor. In contrast, the weight average molecular weight incorporates a weighing factor equal to the molecular weight of the oligomer, which results in the expected values being shifted towards higher molecular weights. A more detailed explanation can be obtained by examining the following equations, used to calculate these molecular weights:

The number average molecular weight is obtained using the following equation:

$$M_n = \frac{\sum_{i=1}^{P} M_i N_i}{\sum_{i=1}^{P} N_i} \tag{26}$$

where M_n is the number average molecular weight, M_i is the molecular weight of an oligomer with i monomers, N_i is the number of polymer species with i monomers, and P is the maximum size of the polymer.

On the other hand, the number average molecular weight is calculated using the following equation:

$$M_w = \frac{\sum_{i=1}^{P} N_i M_i^2}{\sum_{i=1}^{P} N_i M_i} \tag{27}$$

where M_w is the weight average molecular weight of the polymer. It should be noted that in calculating the average molecular weight of polymers, both the numerator and the denominator are weighted by the molecular weight of the polymer chains. This means that higher molecular weight species have a greater impact on the overall molecular weight calculation. As a result, the weight average molecular weight is shifted towards higher values. It is important to keep in mind that this figure is a general representation and may vary depending on the specific polymer system. $\mathrm{M_z}$ is the *z*-average molecular weight, which is another parameter used to characterize the molecular weight distribution of a polymer system, and it is given by the following equation:

$$M_z = \frac{\sum_{i=1}^{P} N_i M_i^z}{\sum_{i=1}^{P} N_i M_i^{z-1}} \tag{28}$$

where z is an index by which the molecular weights are weighed in the calculation of the z-average molecular weight. When $z = 1$, the calculation of M_z reduces to the calculation of the number average molecular weight, M_n. Similarly, when $z = 2$, the calculation of M_z reduces to the calculation of the weight average molecular weight M_w. For higher values of z, the calculation of M_z results in a weighted average that places even greater emphasis on the highest molecular weight species in the sample.

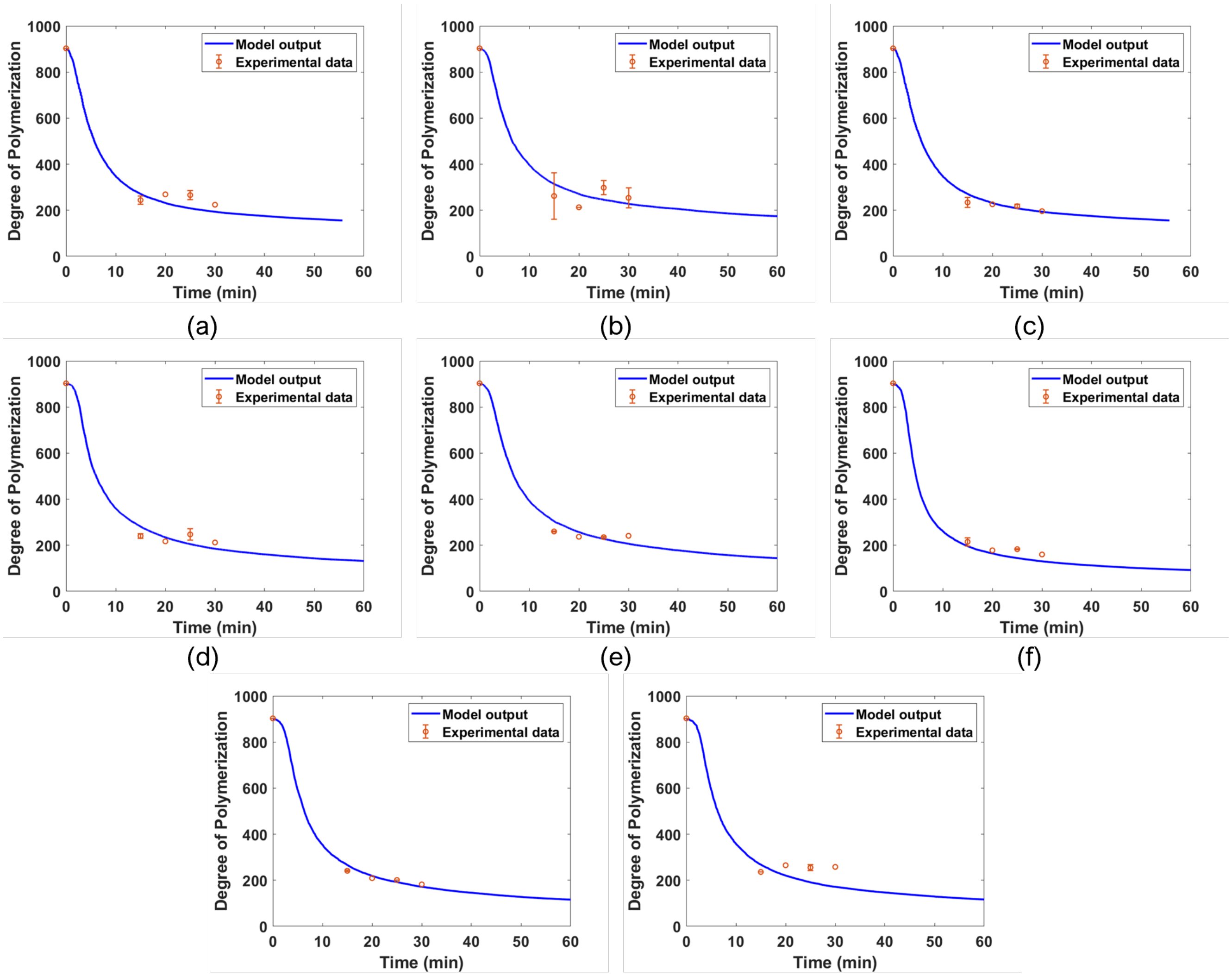

(a) (b) (c) (d) (e) (f) (g) (h)

Fig. 6. Model validation for wood chips with different sizes at different temperatures: (a) 1 mm at 343 K, (b) 3 mm at 343 K, (c) 1 mm at 353 K, (d) 3 mm at 353 K, (e) 5 mm at 353 K, (f) 1 mm at 363 K, (g) 3 mm at 363 K, (h) 5 mm at 363 K.

The activation energies obtained by fitting the experimental data with the model predictions are highlighted in Tables 7-9. Specifically, the energies are listed in the order of high-reactive lignin, low-reactive lignin, cellulose, arabinoxylan, and galactoglucomannan, respectively. An important observation from these tables is that there is an increase in the activation energy barriers (*i.e.*, increased cellulose stability in PSA solvent) with increasing wood chip size.

Table 7. The activation energy of different wood chip thicknesses at 343 K in kJ/mol.

1 μm		3 μm	
E_1	E_2	E_1	E_2
21.75	19.8	24.75	23.7
84.1	23.76	95.7	28.44
24.65	26.4	28.05	31.6
17.4	25.08	19.8	30.02
50.75	110.88	57.75	132.72

Table 8. The activation energy of different wood chip thicknesses at 353 K in kJ/mol.

1 μm		3 μm		5 μm	
E_1	E_2	E_1	E_2	E_1	E_2
26.7	25.5	27.3	26.4	28.5	27.9
103.24	30.6	105.56	31.68	110.2	33.48
30.26	34	30.94	35.2	32.3	37.2
21.36	32.3	21.84	33.44	22.8	35.34
62.3	142.8	63.7	147.84	66.5	156.24

Table 9. The activation energy of different wood chip thicknesses at 363 K in kJ/mol.

1 μm		3 μm		5 μm	
E_1	E_2	E_1	E_2	E_1	E_2
28.5	26.5	31.2	30.00	31.5	30.3
108.2	31.6	120.64	36.00	121.8	36.36
31.3	33	35.36	40.00	35.7	40.4
23.8	31.3	24.96	38.00	25.2	38.38
66.5	142.8	72.8	168.00	73.5	169.68

4.2. Mesoscopic properties

An important application of the model is to predict the temporal variation in the mesoscopic properties of wood chips which otherwise is intricate to measure. To this end, the results in this section are highlighted for wood chips that have CWT of 3.8 μm. It is worth mentioning that the wood chip properties having small values (*e.g.*, CWT) is very difficult to measure, and the proposed high-fidelity model is very useful for the predictions in such cases. The spatiotemporal evolution of the kMC lattice is exhibited in Fig. 7, at the temperature of T = 410 K and the PSA concentration of 72 wt%.

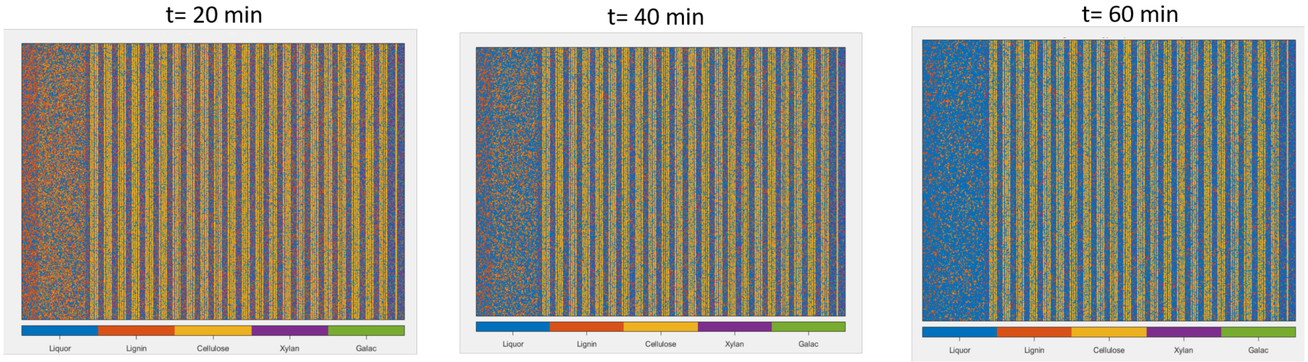

Fig. 7. Spatio-temporal evolution of the kMC lattice during the pulping process at T=410K and PSA concentration of 72 wt%.

In the lattice space, the blue sites represent the entrapped-liquor phase; and the orange, yellow, and purple sites stand for lignin, cellulose, and hemicellulose components in the solid phase, respectively. Once a solid component dissolves, the phase change takes place. Subsequently, these sites are considered to be an entrapped-liquor phase. It is observed that the entrapped liquor content in the wood chips goes up, and the cellulose content and the lignin content in the wood chips fall significantly, implying that the dissolution phenomena lead to the fall in the Kappa number and CWT.

The temporal variation of wood chip properties like the Kappa number and CWT is calculated by varying temperatures. As shown in Fig. 8, the decrease of the Kappa number and CWT is found to become steeper at higher temperatures. The dissolution of the kMC lattice sites from the bulk phase into the solution phase follows an Arrhenius-type equation, with reaction rates increasing significantly at higher temperatures. As a result, the lignin and other components of the wood chips dissolve more rapidly into the free liquor, leading to a sharp decrease in the lignin content and kappa number with increasing temperature. Furthermore, the cell wall thickness (CWT), which depends on the total number of lattice sites present longitudinally, also decreases steeply with increasing temperature.

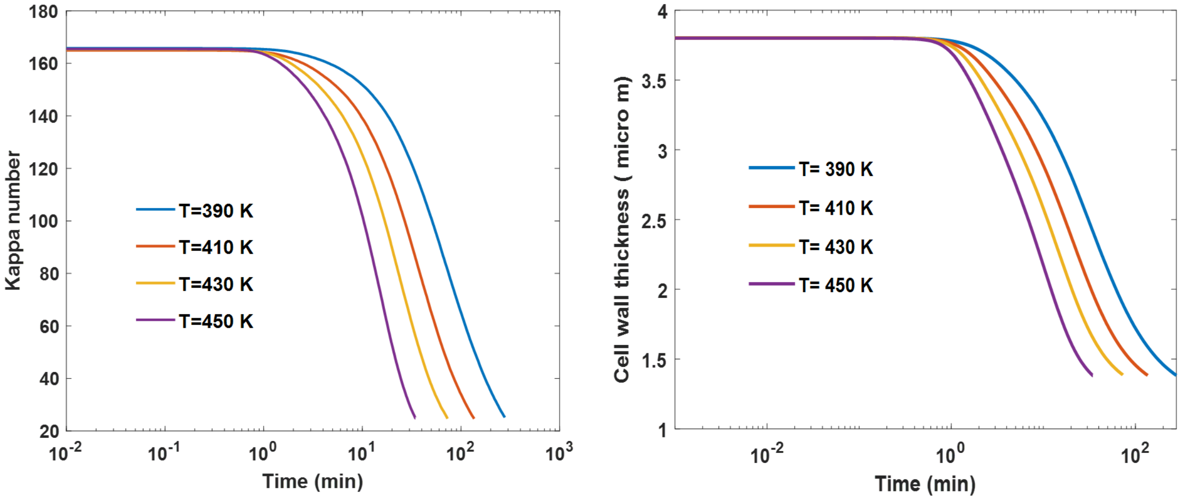

(a) (b)

Fig. 8. Temporal evolution of mesoscopic properties for different temperatures with PSA concentration of 72 wt%: (a) cell wall thickness, and (b) Kappa number.

Additionally, the temporal variation of Kappa number with different PSA concentrations is also exhibited in Fig. 9. It obviously shows that increasing PSA concentration leads to substantial drops in CWT and Kappa number. This is primarily due to the accelerated dissolution rate of the lignin and cellulose resulting from more frequent etching by the solvent.

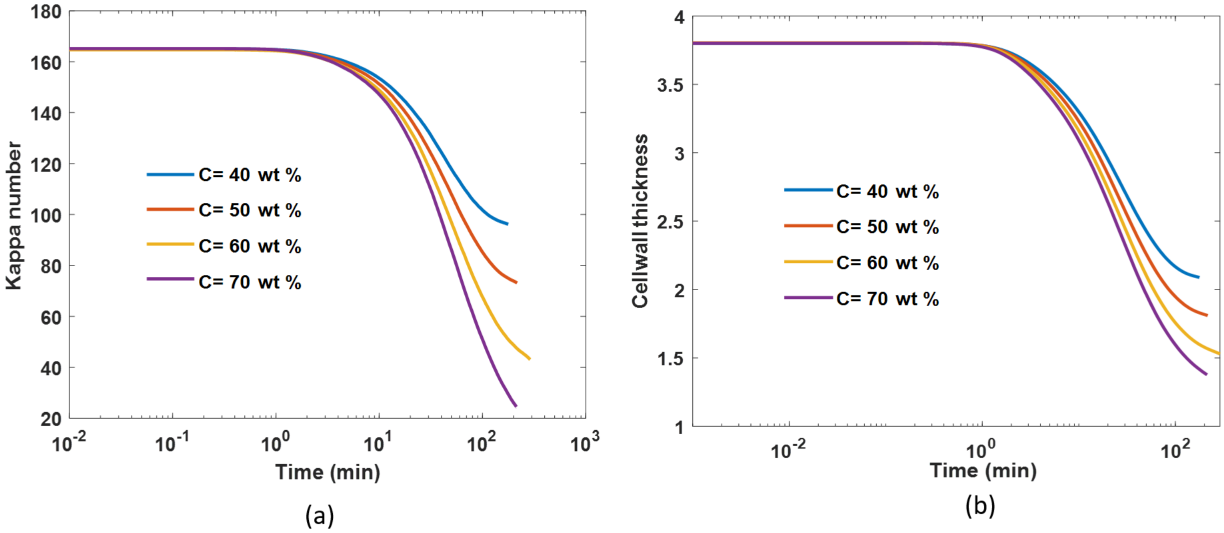

Fig. 9. Temporal evolution of mesoscopic properties at different PSA concentrations for the temperature of 410 K: (a) cell wall thickness, and (b) Kappa number.

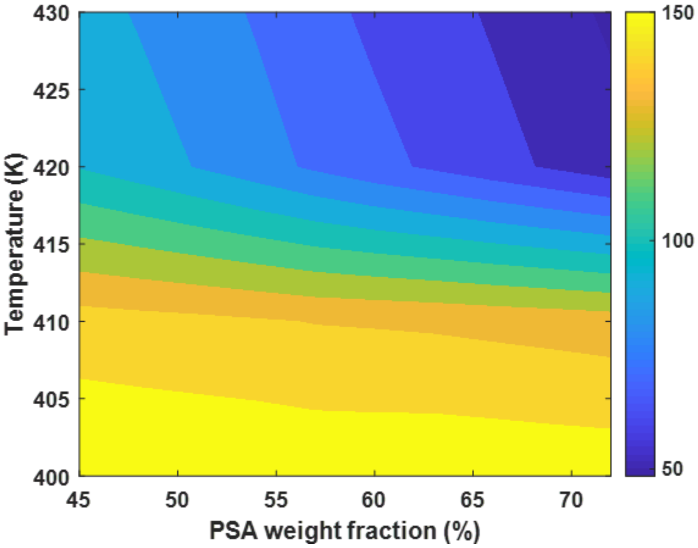

Fig. 10. The sensitivity of Kappa number with varying temperature and PSA weight fraction.

Furthermore, to study the sensitivity of the Kappa number for varying temperatures and PSA concentrations, a three-dimensional plot is obtained in Fig. 10, showing the Kappa number obtained after 100 min of the reaction. The detailed sensitivity analyses aid us to understand how temperature and PSA concentration have a combined impact on the critical mesoscopic property of the wood chips. As expected, the temperature is more influential on these mesoscopic properties than the PSA concentration. This is primarily due to the exponential dependence of the reaction rates on the temperature in the kMC simulations. Obtaining such a plot is useful in providing us with the proper operating conditions.

4.3. Microscopic properties

The microscopic properties like the DP of cellulose are also obtained from the layered-kMC model. Specifically, the model predicts the temporal variation of the DP of cellulose. For demonstration purposes, the temporal evolution of DP of cellulose is presented in Fig. 11.

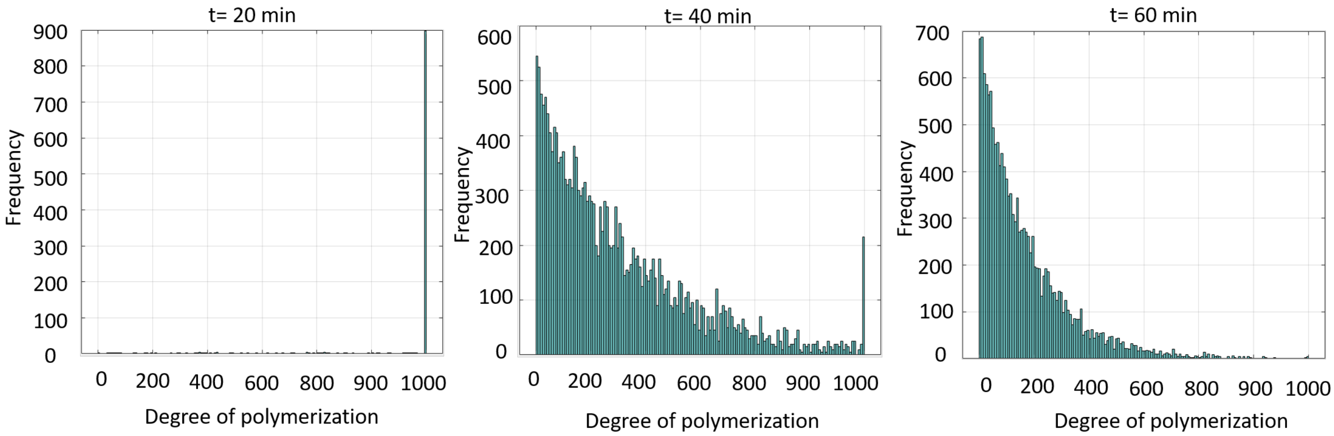

Fig. 11. Temporal evolution of DP for T = 410 K, and PSA concentration of 72 wt%.

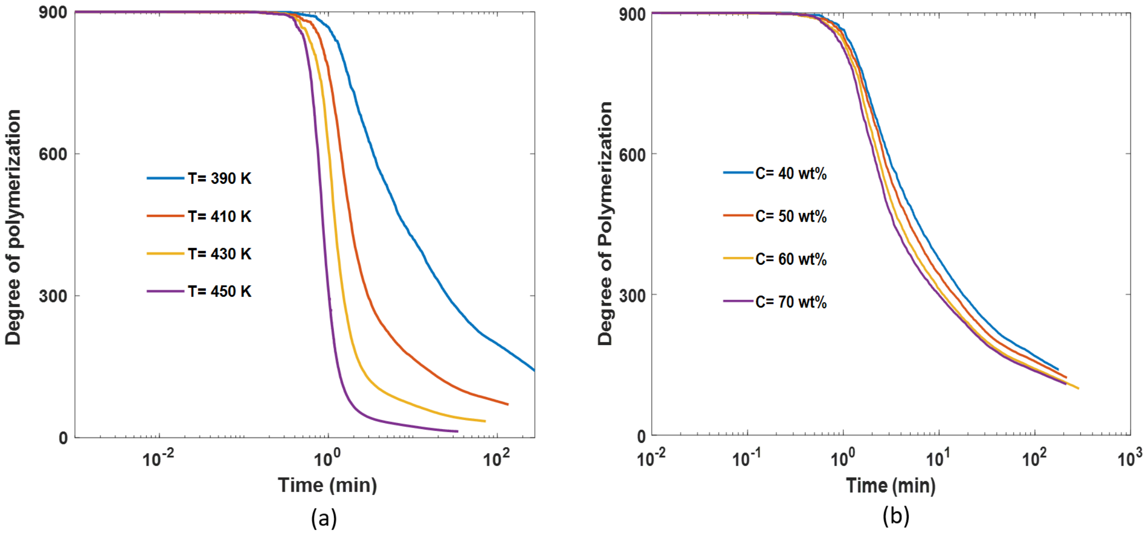

(a)

(b)

Fig. 12. Temporal evolution of DP: (a) varying temperature, and (b) varying PSA concentration.

The variations of the cellulose DP with varying reaction conditions are displayed in Fig. 12, and it is observed that the rate of cellulose degradation increases significantly as the temperature rises. This is primarily accounted for by two important reasons: 1) The increasing temperature accelerates the depolymerization of cellulose nanofibers by hydrolysis of the glycosidic linkages; and 2) It also increases the rate of dissolution of the cellulose. However, it is found that DP changes are far less sensitive to varying PSA concentrations. This is because the PSA concentration does not affect the rate of hydrolysis of the glycosidic linkages but only impacts the rate of dissolution of cellulose. This is an important consequence of the dual mechanisms that play a significant role in the degradation of cellulose nanofibers. The sensitivity plot of the cellulose DP with different temperatures and alkaline conditions is shown in Fig. 13.

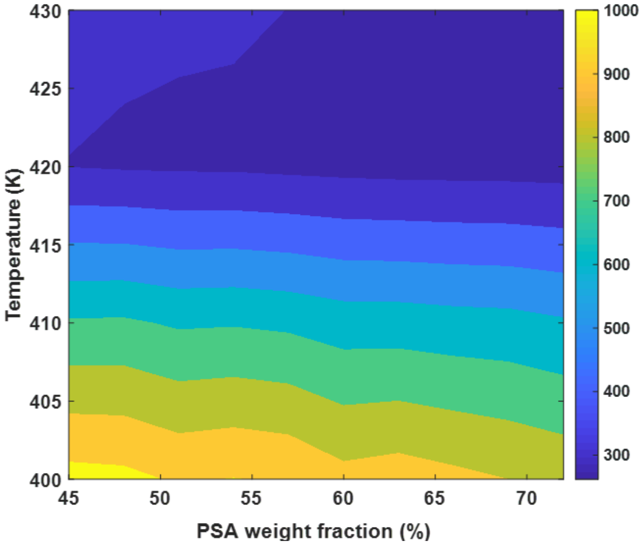

Fig. 13. The sensitivity of the DP with varying temperature and PSA concentration in percentage weight.

In Fig. 13, we examined the effects of PSA concentration and temperature on DP, where our results indicate that increasing PSA fraction and temperature leads to a decrease in DP. In particular, the hydrolysis of the glycosidic linkage remains unaffected by PSA fraction, while dissolution is relatively strongly impacted. As a result, at low PSA concentrations, increasing temperature does not further decrease the DP. This suggests that cellulose degradation occurs less below a certain level of PSA concentration. However, when considering Fig. 10, it is important to note that cellulose fibers resulting from this degradation still exhibit high lignin content.

5. Conclusion

In this work, a layered-kMC simulation was developed to predict the temporal evolution of important mesoscopic properties as well as microscopic properties. In the kMC simulation, the dissolution of wood chips is modeled by considering interactions among the various components in the wood chip and the PSA solvent. The degradation of cellulose nanofibers is modeled via two mechanisms. One is the mechanical detachment of cellulose nanofibers associated with the dissolution of wood chip components, and another is the depolymerization of cellulose nanofibers due to the hydrolysis of glycosidic linkages. The model predictions have good validation with the experimental data at different temperatures. Furthermore, the model was used to observe the temporal evolution of mesoscopic and microscopic properties by varying reaction conditions like temperature and concentration of PSA solvent. The model prediction gives helpful insights into the sensitivity of these properties at various conditions. Also, it should be pointed out that cellulose DP has greater sensitivity to temperature than PSA concentration. This is a result of the two-step process considered here for cellulose nanofiber degradation. Overall, this work, for the first time, captures the cellulose degradation in wood chips and provides useful insights for controlling the cellulose DP. From this viewpoint, this result will greatly assist the paper industries to enhance the paper qualities and then take further steps to resolve present environmental issues.

Declaration of competing interest

The authors declare no competing interest.

Acknowledgments

Financial support from the Artie McFerrin department of chemical engineering and the Texas A&M Energy Institute is gratefully acknowledged. This work was also supported by the National Science Foundation grant CBET2027125.

Literature Cited

[1] W. Sridach, The environmentally benign pulping process of non-wood fibers., Suranaree Journal of Science & Technology 17 (2).

[2] M. S. Sweet, J. E. Winandy, Influence of degree of polymerization of cellulose and hemicellulose on strength loss in fire-retardant-treated southern pine, Holzforschung 53 (3) (1999) 311–317.

[3] A. E. Eneh, S. N. Oluigbo, Mitigating the impact of climate change through waste recycling, Research Journal of Environmental and Earth Sciences 4 (8) (2012) 776–781.

[4] K. U. Kjeldsen, L. Tang, M. G. Jørgensen, K. Ingvorsen, Enumeration and identification of dominant types of sulfate-reducing bacteria in pulp from a paper-recycling plant: a multiphasic approach, FEMS Microbiology Ecology 69 (3) (2009) 481–494.

[5] A. Almasi, M. Mohammadi, A. Azizi, Z. Berizi, K. Shamsi, A. Shahbazi, S. A. Mosavi, Assessing the knowledge, attitude and practice of the kermanshahi women towards reducing,

recycling and reusing of municipal solid waste, Resources, Conservation and Recycling 141 (2019) 329–338.

[6] J. Malešič, I. Kraševec, I. Kralj Cigić, Determination of cellulose degree of polymerization in historical papers with high lignin content, Polymers 13 (12) (2021) 1990.

[7] D. Mboowa, A review of the traditional pulping methods and the recent improvements in the pulping processes, Biomass Conversion and Biorefinery (2021) 1–12.

[8] R. Janzon, J. Puls, A. Bohn, A. Potthast, B. Saake, Upgrading of paper grade pulps to dissolving pulps by nitren extraction: yields, molecular and supramolecular structures of nitren extracted pulps, Cellulose 15 (5) (2008) 739–750.

[9] R. A. Young, Comparison of the properties of chemical cellulose pulps, Cellulose 1 (2) (1994) 107–130.

[10] N. Gurnagul, D. H. Page, M. G. Paice, The effect of cellulose degradation on the strength of wood pulp fibres, Nordic Pulp & Paper Research Journal 7 (3) (1992) 152–154.

[11] S. Lavrykov, B. Ramarao, S. Lindström, K. Singh, 3d network simulations of paper structure, Nordic Pulp & Paper Research Journal 27 (2) (2012) 256–263.

[12] J. Chen, M. Zhang, Z. Yuan, J. Wang, Improved high-yield pulp network and paper sheet properties by the addition of fines, BioResources 8 (4) (2013) 6309–6322.

[13] I. González, S. Boufi, M. A. Pèlach, M. Alcalà, F. Vilaseca, P. Mutjé, Nanofibrillated cellulose as paper additive in eucalyptus pulps, BioResources 7 (4) (2012) 5167–5180.

[14] L. Nilsson, S. Stenström, A study of the permeability of pulp and paper, International Journal of Multiphase Flow 23 (1) (1997) 131–153.

[15] P. Žnidaršič-Plazl, V. Rutar, D. Ravnjak, The effect of enzymatic treatments of pulps on fiber and paper properties, Chemical and Biochemical Engineering Quarterly 23 (4) (2009) 497–506.

[16] J. Jung, H.-K. Choi, S. H. Son, J. S.-I. Kwon, J. H. Lee, Multiscale modeling of fiber deformation: Application to a batch pulp digester for model predictive control of fiber strength, Computers & Chemical Engineering 158 (2022) 107640.

[17] R. De Silva, N. Byrne, Utilization of cotton waste for regenerated cellulose fibres: Influence of degree of polymerization on mechanical properties, Carbohydrate Polymers 174 (2017) 89–94.

[18] S.-j. Kim, J. Jang, Effect of degree of polymerization on the mechanical properties of regenerated cellulose fibers using synthesized 1-allyl-3-methylimidazolium chloride, Fibers and Polymers 14 (6) (2013) 909–914.

[19] L. N. Megashah, H. Ariffin, M. R. Zakaria, M. A. Hassan, Y. Andou, F. N. M. Padzil, Modification of cellulose degree of polymerization by superheated steam treatment for versatile properties of cellulose nanofibril film, Cellulose 27 (13) (2020) 7417–7429.

[20] S. H. Son, H.-K. Choi, J. S.-I. Kwon, Application of offset-free Koopman-based model predictive control to a batch pulp digester, AIChE Journal 67 (9) (2021) e17301.

[21] J. Kim, S. Pahari, J. S.-I. Kwon, Modeling biomass degradation with multiscale kMC simulations, in: Energy Systems and Processes: Recent Advances in Design and Control, AIP Publishing LLC Melville, New York, 2023, pp. 11–1.

[22] P. Shah, H.-K. Choi, J. S.-I. Kwon, Achieving optimal paper properties: A layered multiscale

kMC and LSTM-ANN-based control approach for kraft pulping, Processes 11 (3) (2023) 809.

[23] C. A. Hubbell, A. J. Ragauskas, Effect of acid-chlorite delignification on cellulose degree of polymerization, Bioresource Technology 101 (19) (2010) 7410–7415.

[24] H.-K. Choi, J. S.-I. Kwon, Multiscale modeling and control of kappa number and porosity in a batch-type pulp digester, AIChE Journal 65 (6) (2019) e16589.

[25] H. Choi, J. S. Kwon, Multiscale modeling and multiobjective control of wood fiber morphology in batch pulp digester, AIChE Journal 66 (2020) e16972.

[26] H. Choi, J. S. Kwon, Modeling and control of cell wall thickness in batch delignification, Computers & Chemical Engineering 128 (2019) 512–523.

[27] P. B. Subhedar, P. R. Gogate, Alkaline and ultrasound assisted alkaline pretreatment for intensification of delignification process from sustainable raw-material, Ultrasonics Sonochemistry 21 (1) (2014) 216–225.

[28] C. J. Biermann, Hydrolysis and other cleavages of glycosidic linkages in polysaccharides, in: Advances in Carbohydrate Chemistry and Biochemistry, Vol. 46, Elsevier, 1988, pp. 251–271.

[29] H. Suryanto, E. Marsyahyo, Y. S. Irawan, R. Soenoko, Morphology, structure, and mechanical properties of natural cellulose fiber from mendong grass (fimbristylis globulosa), Journal of Natural Fibers 11 (4) (2014) 333–351.

[30] M. Abdelmouleh, S. Boufi, M. N. Belgacem, A. Dufresne, A. Gandini, Modification of cellulose fibers with functionalized silanes: effect of the fiber treatment on the mechanical

performances of cellulose–thermoset composites, Journal of Applied Polymer Science 98 (3) (2005) 974–984.

[31] D. Maldas, B. Kokta, C. Daneault, Influence of coupling agents and treatments on the mechanical properties of cellulose fiber–polystyrene composites, Journal of Applied Polymer Science 37 (3) (1989) 751–775.

[32] S. H. Son, H.-K. Choi, J. Moon, J. S.-I. Kwon, Hybrid Koopman model predictive control of nonlinear systems using multiple EDMD models: An application to a batch pulp digester with feed fluctuation, Control Engineering Practice 118 (2022) 104956.

[33] H.-K. Choi, S. H. Son, J. S.-I. Kwon, Inferential model predictive control of continuous pulping under grade transition, Industrial & Engineering Chemistry Research 60 (9) (2021) 3699–3710.

[34] B. B. Hallac, A. J. Ragauskas, Analyzing cellulose degree of polymerization and its relevancy to cellulosic ethanol, Biofuels, Bioproducts and Biorefining 5 (2) (2011) 215–225.

[35] R. Funahashi, Y. Ono, R. Tanaka, M. Yokoi, K. Daido, T. Inamochi, T. Saito, Y. Horikawa, A. Isogai, Changes in the degree of polymerization of wood celluloses during dilute acid hydrolysis and tempo-mediated oxidation: Formation mechanism of disordered regions along each cellulose microfibril, International Journal of Biological Macromolecules 109 (2018) 914–920.

[36] M. Andersen, C. Panosetti, K. Reuter, A practical guide to surface kinetic monte carlo simulations, Frontiers in Chemistry 7 (2019) 202.

[37] S. Pahari, B. Bhadriraju, M. Akbulut, J. S.-I. Kwon, A slip-spring framework to study

relaxation dynamics of entangled wormlike micelles with kinetic monte carlo algorithm, Journal of Colloid and Interface Science 600 (2021) 550–560.

[38] D. He, Y. Wang, C. G. Yoo, Q.-J. Chen, Q. Yang, The fractionation of woody biomass under mild conditions using bifunctional phenol-4-sulfonic acid as a catalyst and lignin solvent, Green Chem. 22 (2020) 5414–5422.

[39] M. Poletto, H. L. Ornaghi Junior, A. J. Zattera, Native cellulose: structure, characterization and thermal properties, Materials 7 (9) (2014) 6105–6119.

[40] A. Sluiter, B. Hames, R. Ruiz, C. Scarlata, J. Sluiter, D. Templeton, D. Crocker, Determination of structural carbohydrates and lignin in biomass, Laboratory Analytical Procedure 1617 (1) (2008) 1–16.

[41] C. M. S. da Silva, B. R. Vital, O. C. Angélica de Cássia, E. V. Costa, M. A. de Magalhães, P. F. Trugilho, Structural and compositional changes in eucalyptus wood chips subjected to dry torrefaction, Industrial Crops and Products 109 (2017) 598–602.

[42] B. Grisogono, D. BelusŠIĆ, A review of recent advances in understanding the mesoand microscale properties of the severe bora wind, Tellus A: Dynamic Meteorology and Oceanography 61 (1) (2009) 1–16.

[43] T. Christensen, A mathematical model of the kraft pulping process, Purdue University, 1982.

[44] H. Choi, J. S. Kwon, Multiscale modeling and control of Kappa number and porosity in a batch pulp digester, AIChE Journal 65 (6) (2019) e16589.

[45] E. Agosin, R. A. Blanchette, H. Silva, C. Lapierre, K. R. Cease, R. E. Ibach, A. R. Abad, P. Muga, Characterization of palo podrido, a natural process of delignification in wood, Applied and Environmental Microbiology 56 (1) (1990) 65–74.

[46] S. R. Chandrasekaran, P. K. Hopke, L. Rector, G. Allen, L. Lin, Chemical composition of wood chips and wood pellets, Energy & Fuels 26 (8) (2012) 4932–4937.

[47] S. H. Son, H. Choi, J. S. Kwon, Multiscale modeling and control of pulp digester under fiber-to-fiber heterogeneity, Computers & Chemical Engineering 143 (2020) 107117.

[48] P. A. Wisnewski, F. J. Doyle III, F. Kayihan, Fundamental continuous-pulp-digester model for simulation and control, AIChE journal 43 (12) (1997) 3175–3192.

[49] L. Van Loon, M. Glaus, Review of the kinetics of alkaline degradation of cellulose in view of its relevance for safety assessment of radioactive waste repositories, Journal of Environmental Polymer Degradation 5 (1997) 97–109.

[50] U. Hirn, R. Schennach, Comprehensive analysis of individual pulp fiber bonds quantifies the mechanisms of fiber bonding in paper, Scientific Reports 5 (1) (2015) 1–9.